

Analysis of SiC and SiC-Cascode MOSFET in the design of power electronics converters for more electric aircrafts

Osmar Felipe Alves Eleodoro, Vitor Fonseca Barbosa, Gustavo B. Lima, Luiz Carlos Gomes Freitas

Faculty of Electrical Engineering, Federal University of Uberlândia, Uberlândia, Brazil

Article Info

Article history:

Received Jun 25, 2022

Revised Aug 11, 2022

Accepted Aug 29, 2022

Keywords:

DC distribution

Microgrids

More-electric aircraft

Power electronics

Silicon carbide

Wideband gap semiconductors

ABSTRACT

Wideband gap (WBG) semiconductors have developed rapidly in recent years, enabling greater efficiency and power density in the design of power electronics converters for several areas of application. In this sense, this work analyzes the efficiency and specificities of silicon carbide (SiC) technologies and their cascode topology (SiC-Cascode), operating at high switching frequencies. The analyzes are performed using a Boost converter designed for conversion systems in the more-electric aircraft (MEA) context, where the alternating current (AC) power systems can operate at fixed frequency (115 V/400 Hz), or at variable frequency (115 V/360-800 Hz), such as observe in Boeing 787, and the direct current (DC) power system can operate with a DC bus of 400 V and ± 270 V are normally used. To validate the project, computer simulations were performed and a 1.0 kW prototype was built in the laboratory. The performance analyses demonstrates that 97.5% of efficiency is achieved at 500 kHz switching frequency.

This is an open access article under the [CC BY-SA](https://creativecommons.org/licenses/by-sa/4.0/) license.



Corresponding Author:

Luiz Carlos Gomes Freitas

Faculty of Electrical Engineering, Federal University of Uberlândia

Av. João Naves de Ávila, 2121, Campus Santa Mônica – Bloco 3N, CEP 38400-902, Uberlândia, Brazil

Email: lcgfreitas@ufu.br

1. INTRODUCTION

The material traditionally applied for semiconductor purposes in power electronics converters is silicon (Si), which was discovered at the end of the 19th century and has been dominant ever since, due to its large consumer market and technology widely disseminated at industrial level [1]. Currently, several material technologies besides Si are applicable in semiconductor devices. Some examples available on the market are the silicon carbide (SiC) and gallium nitride (GaN), which are used in high-performance, wideband gap (WBG) switching elements. The use of the above-mentioned materials, although initially costly, has developed rapidly, seeking to reach the theoretical limits of each material.

Recent technologies of Si, SiC and GaN technologies have a higher energy band and breakdown voltage enabling the creation of high voltage and WBG devices [2], [3]. Due to the high switching speed of WBG devices, it is possible to increase the switching frequencies and to reduce the switching losses, leading to greater energy savings. Additionally, it is possible to reduce the volume and weight of the passive elements used, drastically reducing the amount of raw material needed to make the final product. The gain with energy savings is considerable, offsetting the initial investment during its lifetime, even with an initial higher cost when compared to the implementation of Si semiconductors [4], [5]. However, with the advances in the semiconductor industry, this investment has been reduced enabling greater profitability in the application of WBG semiconductors also in the short term [6]. Despite the advantages of WBG technologies, the high switching frequencies, added to the high power processing levels, can accentuate the EMI [2], [7],

[8]. Several previous studies reported in [4], [5], [9]–[15] prove the effective gain in performance when WBG semiconductor devices are applied in power electronics converters, encouraging their increasing application in the industrial and academic environment. Additionally, recent studies concerning the deployment of SiC [16]–[21] and GaN [22], [23] technologies in several applications, the latter being used in high-power devices, as reported in [24].

Currently, SiC technology moves to the preponderant position in high power applications since it presents greater thermal conduction among the mentioned technologies, together with greater availability in the market. This technology is already found in different devices, such as MOSFETs and JFETs, and in the form of hybrids technologies, such as SiC-Cascode, originated from the use of combined SiC-JFET and Si-MOSFET devices [25], which presents the advantages of simplified Si triggering, combined with the high bandwidth of the SiC-JFET device. The technology begins to gain space in the market, being applied to high-power modules by several manufacturers, in addition to being widely discussed in the academic context as a superior alternative to Si. It has an intermediate price, with transistors accessible to the industry and to the final consumer. Therefore, the evaluation of SiC-based semiconductor technologies in their practical limits is encouraged, aiming at greater efficiency and higher power density from the increase in the switching frequency. Such characteristics form the basis of requirements for embedded applications, such as found in electric vehicles (EV) and more-electric aircraft (MEA) [26]–[29]. Applied to diodes, they are present in devices with zero reverse recovery current and zero forward recovery voltage, which inhibits power losses due to switching in passive devices [30].

Focusing on more-electric aircraft, in [27] the authors presented an important study evidencing that the search for improvements in electrical converters is the key to systems with high efficiency and reliability. Thus, the use of new semiconductor technologies (SiC and GaN) helps in the performance of these converters, which are influenced by harsh environment, low pressures and cosmic radiation present at high altitudes. In order to illustrate what has been exposed, Figure 1, which was originally presented in [27], shows the main requirements and trends that must be analyzed in electronic converter designs for MEA applications. Figure 2 indicates that the use of SiC-MOSFET and GaN-HEMT, with switching frequencies in the range of 100 kHz to around 300 kHz, are the best choice.

Marroqui *et al.* [31] presented a comparative study between SiC MOSFET and SiC-Cascode in the scope of robustness in short-circuit conditions. Both technologies were capable of with-standing 3 μ s events and showed little variation in their parameters after 200 occurrences of this type. Zhao *et al.* [32] presented the semiconductor suitability for parallel operation has been evaluated and the selected SiC-MOSFET device presented the highest efficiency in current division, from a double pulse test, at a continuous voltage of 400 V and inductive load of 150 μ H. Martin *et al.* [33] their performance on the implementation of a high-power inverter (100 kW), operating at a fixed switching frequency of 50 kHz has been analyzed. The SiC-Cascode technology presented greater efficiency and provided higher power density. These studies have shown comparisons between the technologies of semiconductors only on a restricted scale, emphasizing specific operational characteristics and at predetermined switching frequencies.

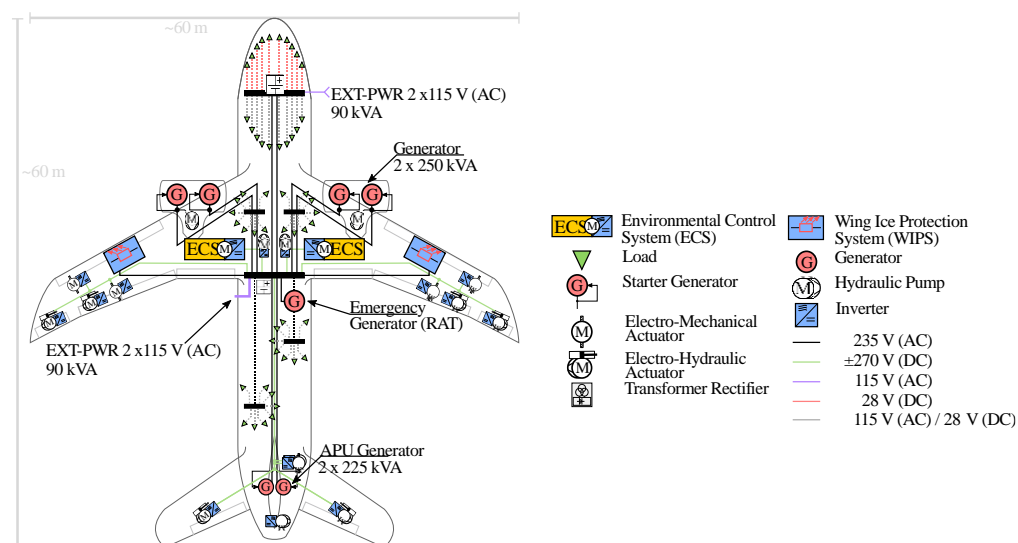


Figure 1. Electric schematic of MEA—adapted from [27]

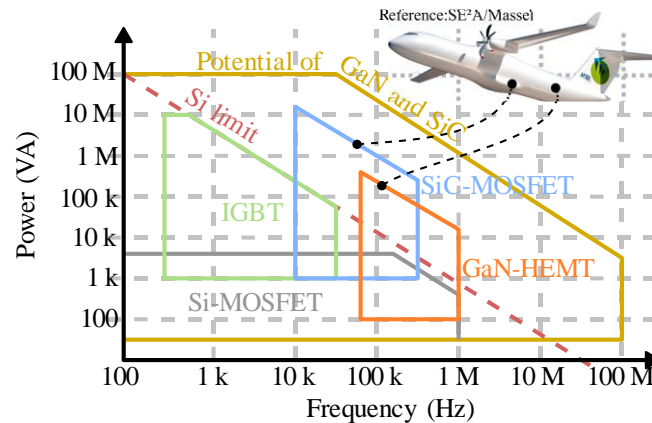


Figure 2. Semiconductors typical application–adapted from [27]

In this scenario, the article proposed herein presents a study concerning the performance analysis of Boost converter operating as Front-end converter for Power Factor Correction (PFC) and also as DC-DC converter for electronics loads, both in the MEA context, where the Alternating Current (AC) power systems can operate at fixed frequency (115 V/400 Hz), or at variable frequency (115 V/360-800 Hz), such as in Boeing 787, and the direct current (DC) power system can operate with a DC bus of 400 V and ± 270 V are normally used. To validate the project, computer simulations were performed and a 1.0 kW prototype was built in the laboratory. The performance analyses demonstrates that 97.5% of efficiency is achieved at 500 kHz switching frequency. To present the obtained results, the remainder of this article is structured as follows. Section 2 describes the proposed power electronics converter for carrying out the simulation and experimental tests, including its design procedure and control strategies. Section 3 details the methodology used for efficiency analysis; and finally, the concluding remarks are elucidated in Section 4.

2. IMPLEMENTATION OF A SiC AND SiC-CASCODE BASED BOOST CONVERTER

In order to analyze the applicability of high frequency systems for high power density power electronics converters, which is essential for embedded systems such as MEA applications, the performance of the Boost converter is evaluated under switching frequency varying from 50 kHz to 1300 kHz. The control algorithm was developed in C language and embedded in the multi-core DSP TMS320F28379D from Texas Instruments. For DC-DC conversion system, the Boost topology is portrayed in Figure 3, and the parameters of the experimental set-up are described in Table 1. The system contains protection devices against voltage surges (varistor) and overcurrent (fuse). Additionally, an overcurrent protection was implemented via software and is based on tripping aid sent by the current sensor, assuring safety and reliability under short-circuit occurrence. For the AC-DC conversion system, a Graetz bridge rectifier is added at the input of the circuit, with the other parameters unchanged. The average current mode control technique was implemented via software in the DSP. The AC input voltage is 220 V_{RMS} at frequencies varying from 400 Hz to 800 Hz, as found in MEA's electric power systems (EPS).

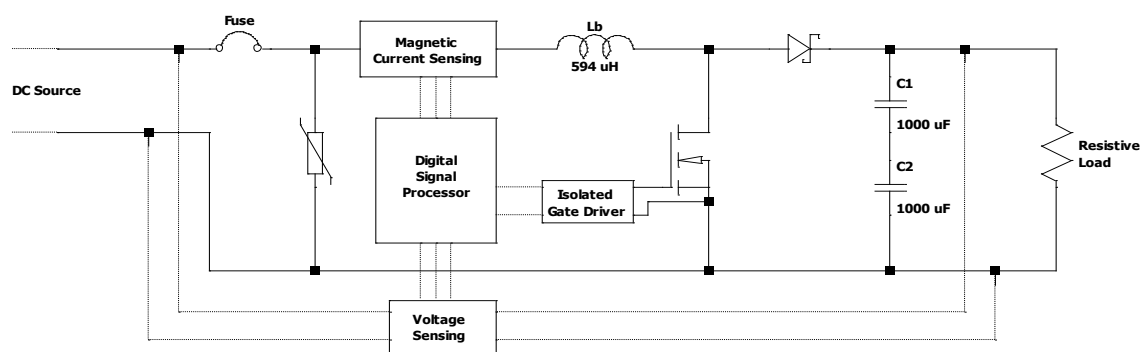


Figure 3. Boost converter for AC-DC operation (with a Graetz bridge rectifier added at the input) and for DC-DC operation (without a Graetz bridge)

Considering the application in high voltage and high switching frequencies, optimization criteria based on reference designs made available by semiconductor manufacturing companies (Cree, Texas Instruments, United SiC, among others) were implemented for the PCB. An isolated DC-DC converter for the gate driver was also added to the circuit board, reinforcing the galvanic isolation between the control circuits and the power circuit. Other components were powered by dedicated integrated circuits implemented in the PCB. The final board kept dimensions of 100×100 mm, with semiconductor devices kept at the bottom of the board providing better connection to the heatsink.

Table 1. Parameters of the Boost converters implemented in laboratory

Parameter	DC-DC conversion	AC-DC conversion
Rated power [W]	1000	1000
Input voltage	200 V_{DC}	220 V_{RMS} - 400 Hz to 800 Hz
Output voltage [V]	400	400
Capacitor C_B ¹ [μF]	500	500
Inductor L_b [μH]	594	594
$R_{ESR(C)}$ ¹ [mW]	300	300
Resistive load [W]	160	160
Diode	C3D10065A	C3D10065A
Switches	C3M0120100K UF3C120150K4S	C3M0120100K UF3C120150K4S
Switching frequency	200 kHz	200 kHz
Inductor physical specification		
Core material	TDK SIFERRIT N97	TDK SIFERRIT N97
Core	PQ 50/50	PQ 50/50
Gap [mm]	~1	~1
Gap Material	Paper	Paper
$R_{ESR(L)}$ [mW]	37	37
Turns	45	45
Wire	AWG 18 x 2	AWG 18×2
Gate driver parameters		
$R_{G(on)}$ [W]	10	11.7
$R_{G(off)}$ [W]	3.2	23.5
$C_{GS(ext)}$ [pF]	1000	1000

¹Values related to the equivalent total capacitance

In the literature, numerous control strategies applicable to power electronics converters are found, including from simplified controls based on hysteresis or pulse width modulation (PWM) [34], [35], to asymmetric PWM controllers [36] and the use of multi-objective optimization algorithms [37]. Among the strategies applicable to AC-DC conversion systems, there is the average current mode control technique [38], which was implemented in this work to control voltage and current simultaneously, in order to impose input line current with low total harmonic distortion (THDi), which is a crucial indicator in electrical power quality indicators in power electronics systems [39]. A sinusoidal voltage reference signal synchronized with the input voltage is also needed to assure unitary power factor. This is made deploying a second order generalized integrator - phase locked loop (SOGI-PLL) [40], which filters potential noise and input voltage distortions. The system bandwidth must be low, so as not to interfere with the waveform imposed by SOGI-PLL at the input current. A first-order low-pass filter was also deployed in the voltage feedback to attenuate the current ripple caused by DC-bus voltage ripple at the input voltage frequency.

For the design of the controllers, the converter transfer function is required for small disturbances in the duty cycle. From the average model in the state-space, the plant was raised, described in (1) for the output voltage, and in (2) for the input current. The parameters used referred to the design values, with an average duty cycle of 0.5 and load resistance of 160 Ω.

$$G_1(s) = \frac{\widehat{v}_o(s)}{\widehat{d}(s)} = \frac{-1 \times 10^4 s^3 + 6.721 \times 10^8 s^2 + 9.537 \times 10^{-5} s + 5.649 \times 10^{14}}{s^4 + 25 s^3 + 1.681 \times 10^6 s^2 + 2.101 \times 10^7 s + 7.062 \times 10^{11}} \quad (1)$$

$$G_2(s) = \frac{\widehat{i}_m(s)}{\widehat{d}(s)} = \frac{6.723 \times 10^5 s^3 + 2.521 \times 10^7 s^2 + 5.651 \times 10^{11} s + 1.412 \times 10^{13}}{s^4 + 25 s^3 + 1.681 \times 10^6 s^2 + 2.101 \times 10^7 s + 7.062 \times 10^{11}} \quad (2)$$

Using MATLAB software, the PI controllers were designed from the closed loop frequency response. Each controller has its estimated bandwidth according to the switching frequency and the input voltage frequency (estimated bandwidth greater than 10–100 times the input voltage frequency and less than

1/10 of the switching frequency, approximately, for the current controller; and at least 10 times lower bandwidth for the voltage controller).

In (3) and (4) are found the transfer functions of the applied PI controllers, for the control of current and voltage, respectively, in the frequency domain. Controller C_1 refers to the current loop compensation, found in the internal control loop, while controller C_2 refers to the external PI controller, after voltage feedback, both shown in Figure 4.

$$C_1(s) = 0.16745 \left(\frac{s + 7.507 \times 10^4}{s} \right) \quad (3)$$

$$C_2(s) = 0.094203 \left(\frac{s + 44.42}{s} \right) \quad (4)$$

For the application in the discrete-time domain, from the DSP, the controllers C_1 and C_2 if were emulated, using the Tustin method. The method maintains its transient characteristics as previously designed [41], only varying the sampling frequency in the emulation process, which depends on the switching frequency of the converter. The block diagram illustrating the implemented control strategy in Figure 3 and the power circuit shown in Figure 4 were validated using PSIM software. In Figure 5, for a load step from 0.5 pu to 1 pu (320 Ω to 160 Ω of load), a voltage undershoots of approximately 5% and an accommodation time (1%) of about 70 ms were measured, with imposition of sinusoidal current with low harmonic distortion (THDi < 5% for rated load), validating the designed control. As an example, in Figure 5 it is noted that the DC voltage at the output of the Boost converter suffers little variation due to the action of the voltage and current controllers. For operation at 400 Hz and 800 Hz, the bandwidth of the PI controllers does not satisfy the operating conditions for switching frequencies below 100 kHz. The respective experimental results will be presented in section 4.

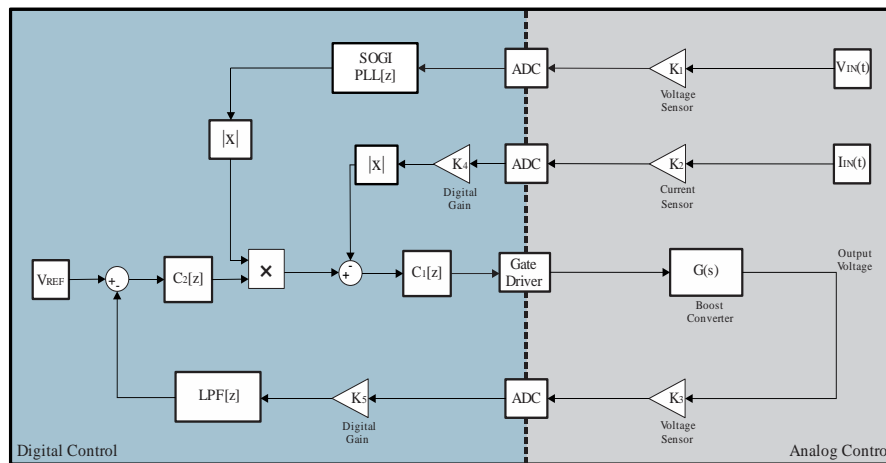


Figure 4. Experimental and simulation control setup

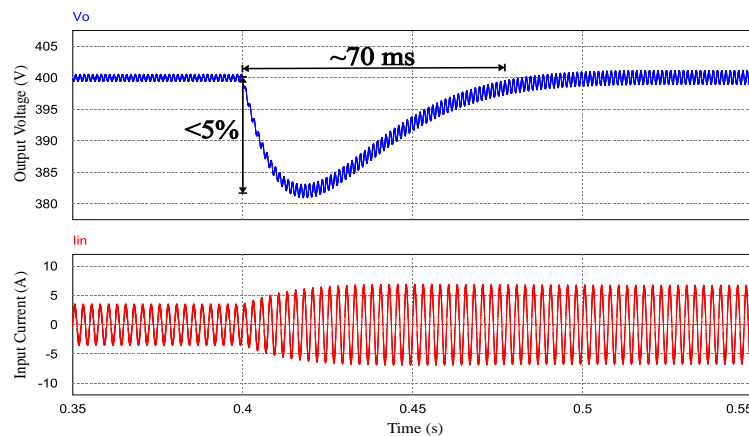


Figure 5. Simulation result for a load step at 400 Hz from 50% to 100% of rated power

3. LOSSES ANALYSIS FOR THE IMPEMETED BOOST CONVERTERS

Regarding the losses in power electronics converters, it is possible to highlight the conduction losses, switching losses and magnetic losses. Leakage losses, although they exist, do not contribute significantly to the studies carried out, so they will be disregarded. The device's parameters used are usually found in their datasheet, and in some cases, they must be measured from laboratory tests, as in the case of the inductor series resistance $R_{ESR(L)}$. The conduction power losses in switched circuits can be estimated from the resistance of the elements used, as well as from the current circulating in the circuit to be analyzed, with the exception of diodes, which also depend on their forward bias voltage. The other power conduction losses, such as in the PCB tracks or in connection cables, have a reduced contribution (complementary losses) and will not be addressed in the proposed analysis. Therefore, the conduction power losses in a FET device can be expressed as (5).

$$P_{cond(s)}(t) = R_{DS(on)}(T_j)i_s^2(t) \quad (5)$$

here, i_s is the instantaneous drain current, $R_{DS(on)}$ is the resistance between drain and source in the on state and T_j is the junction temperature of the transistor.

Switching losses occur during semiconductor state transitions, being characterized by the superposition between voltage and current at this instant. As the number of transitions is directly proportional to the switching frequency, switching losses also have the same characteristic. However, switching losses have greater modeling complexity, requiring the contribution of several studies in order to develop a model that is close to the one found in practice. Prado *et al.* [42] presented an analytical model for MOSFETs suitable for this application, therefore, it was used in the proposed paper. Therefore, losses for MOSFETs can be given by (6).

$$P_{sw(s)} = \frac{1}{2}(t_{on}I_{on} + t_{off}I_{off})f_{ch}V_{DS} \quad (6)$$

where $P_{sw(s)}$ represents the switching power dissipation in the MOSFET, t_{on} and t_{off} are the overlap times in the transitions for conduction and blocking respectively, I_{on} and I_{off} are the input and output switching currents, f_{ch} is the switching frequency and V_{DS} is the blocking voltage at the switch.

To determine the overlap times, is necessary to determine the charging and discharging behavior of the gate-source capacitance (C_{GS}) and gate-drain capacitance (C_{GD}). The modeling of the gate-source load (Q_{GS}) is given by (7) and is based on the input capacitance (C_{ISS}) of the MOSFET, the gate threshold voltage (V_{TH}) and the gate plateau voltage (V_{PL}).

$$Q_{GS} = C_{ISS}(V_{PL} - V_{TH}) \quad (7)$$

For the gate-drain load model (Q_{GD}), the study becomes complex due to the non-linearities of C_{GD} with the variation of the blocking voltage. From [42] one can conclude that a valid gate-drain load model (Q_{GD}) can be found using (8), and takes into account only two points of the capacitance curve $C_{GD} \times V_{DS}$ found in the datasheet. The determination of point A was associated with the time constant of RC circuits (τ) representing the voltage drop of V_{DS} in 2τ , where the voltage reaches 13.5 % of V_{DS} . The proposed method is based on a linearization between the voltages of points A and B ($0.135 \times V_{DS}$ and V_{DS} , respectively), resulting in the approximation by the area of a triangle, equivalent to the capacitance charge C_{GD} .

$$Q_{GD} = \frac{C_{GD(B)}V_{DS} + C_{GD(A)}0.135V_{DS}}{2} \quad (8)$$

$$Q = Q_{GS} + Q_{GD} \quad (9)$$

Knowing the two contributions to the total gate-source load, the total load (Q) required to activate the switch is reached according to (9).

For the calculation of the overlap times, the gate currents for charging (I_{Gon}) and discharging (I_{Goff}), still necessary, which require the internal gate resistors (R_{Gint}), for switching on (R_{Gon}) and for switching off (R_{Goff}), as given by (10) and (11).

$$I_{Gon} = \frac{V_{DR} - V_{PL}}{R_{Gon} + R_{Gint}} \quad (10)$$

$$I_{Goff} = \frac{V_{PL}}{R_{Goff} + R_{Gint}} \quad (11)$$

Finally, the overlap times t_{on} e t_{off} can be calculated from (12) and (13), which are used in (6) to determine the switching losses.

$$t_{on} = \frac{Q}{I_{Gon}} \quad (12)$$

$$t_{off} = \frac{Q}{I_{Goff}} \quad (13)$$

The switching losses referred to the diode are related to reverse recovery. Therefore, due to the use of SiC technology devices, which present zero reverse recovery charge, it will be disregarded in this paper. For the inductor, the core losses are dependent on the variation of magnetic flux, temperature, and the switching frequency imposed on the device. According to the material used, curves that determine the volume losses (P_v) of the material can be presented by the manufacturers, according to the indicated parameters. Losses are generally given in kW/m³, and are presented for discrete values of magnetic flux variation. According to [43], the variation of magnetic flux for inductors (ΔB) is given by (14), where N is the number of turns, ΔI_L is the current ripple in the inductor, l_g is the gap length, MPL is the mean magnetic path length and μ_m is the relative magnetic permeability of the material.

$$\Delta B = \frac{0.4\pi N \frac{\Delta I_L}{2} 10^{-2}}{l_g + \left(\frac{MPL}{\mu_m}\right)} \quad (14)$$

$$P_{core} = P_v VOL_L \quad (15)$$

From the data collected, the inductor loss is calculated using (15), where P_{core} is the power dissipated in the magnetic core, and VOL_L is the inductor volume given in m³.

For DC-DC conversion, the analysis of power losses will be performed using switching frequencies between 100 kHz and 500 kHz, corresponding to the typical and borderline frequency for SiC technology, seen in Figure 2. The analysis will be carried out in order to consider the sources of losses and indicate possible points for improving the overall efficiency, making it possible to achieve greater efficiency and power density for embedded applications, as in the MEA context. Operating temperature of 100°C is considered for the determination of power losses in the MOSFETs (SiC and SiC-Cascode), and 40°C is considered for the rest of the circuit. Using the mathematical procedure described in the last section it is possible to quantify the power losses and also identify the mains sources of power in power electronics converters.

As portrayed in Figure 6, for a switching frequency of 100 kHz, the current ripple in the inductor is higher, causing significant losses in the magnetic core, which is equivalent to 30% of the total losses. The switching power losses at this frequency correspond to 16% (13.62 W). For 500 kHz switching frequency, the core losses are drastically reduced, as a consequence of the lower current ripple and magnetic flux in the inductor. Hence, they are responsible for only 1% of the total losses. In contrast, switching losses are dominant, equivalent to 61%. The conduction losses found have little variation, since the analysis is performed under the same load condition.

For SiC-Cascode, the results obtained are illustrated in Figure 7. The main differences are found in the semiconductors where the power switching loss and the power conduction loss are lower using SiC-Cascode device. For 100 kHz switching frequency, the power switching losses are equivalent to only 10% of the total power loss; while at 500 kHz, the total power loss is equivalent to 42%, with linear growth as the switching frequency increases. Even though the same inductor is used in both experiments, one must observe that the losses in the magnetic material were reduced from 30% to only 2% of the total. This is due to the fact that the current ripple is considerably reduced in higher switching frequencies. The total power loss at switching frequencies of 100 kHz and 500 kHz are 13.87 W and 14.84 W respectively. The reduction in the power switching losses is due to the simplification of the transistor's drive characteristics, which has higher V_{TH} and lower V_{PL} , leading to a shorter current transition period and waveforms overlap. The V_{PL} voltages measured for SiC device was 9.5 V and 6.52 V for SiC-Cascode device. In this context, it is important to emphasize that this operational characteristic together with the intrinsic capacitances, dictate the switching speeds, directly affecting the bandwidth of the transistor. Therefore, special attention must be dedicated when choosing FETs for designs with high switching frequency.

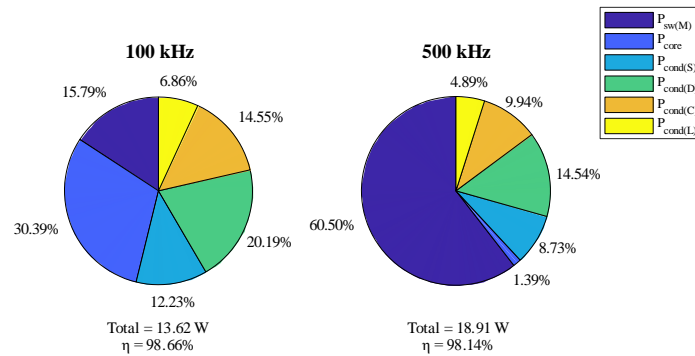


Figure 6. Power losses analysis with SiC device for rated power (1 kW)

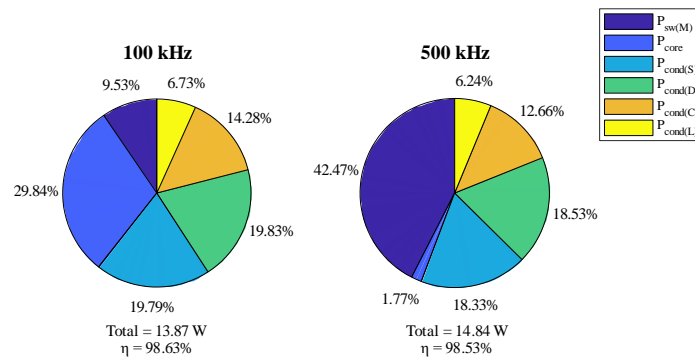


Figure 7. Power losses analysis with SiC-cascode device for rated power (1 kW)

4. EXPERIMENTAL RESULTS AND DISCUSSIONS

Figure 8 shows the laboratory prototype. The connections between the control and power circuits were made from shielded cables to mitigate electromagnetic interference. The connection of external components, such as voltage sensors, protection devices, inductor and bridge rectifier were made from ordinary cables. For heat dissipation, an aluminum heatsink is used at the bottom of the power circuit. The converter performance was tested in two operating situations: DC-DC conversion and AC-DC conversion at varying frequency of 400-800 Hz, as found in MEA. The results were obtained in steady state, with stable operating temperature according to the load and switching frequency. For all operating conditions, the input voltage was applied by a controlled voltage source in order to mitigate injected noise and maintain harmonic distortion levels without interference from external factors. The efficiency measurements refer to the input and output powers of the power circuit, disregarding losses related to gate-driver and control circuits. In this section, the results obtained for both operating conditions will be discussed, seeking to highlight the main advantages provided by the semiconductors technologies used and their potential for MEA application.

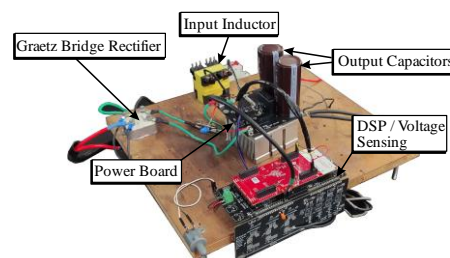


Figure 8. Prototype developed in laboratory

4.1. DC-DC conversion system for MEA

For the DC-DC conversion system, the input and output powers of the experimental were measured using a precision equipment - YOKOGAWA WT230. The switching frequency was set from 50 kHz to

1300 kHz. The maximum switching frequency was chosen regarding the maximum power dissipation of 50 W, which is reached at switching frequency of 1300 kHz, at rated power. The waveforms presented were measured using the TEKTRONIX MDO3034 and MDO4054-3 oscilloscopes, using isolated voltage probes, in order to mitigate external noise. For reasons of safety and susceptibility to mutual interference between the control and power systems, in conjunction with operation at the practical limits of the semiconductors, the DC-DC operation will be driven in open loop. However, small adjustments are made according to the operating frequency in order to keep the gain constant. From the data obtained, it is observed that the SiC-Cascode MOSFET technology provided greater efficiency with switching frequency of 100 kHz, as illustrated in Figure 9. Initially, both technologies proved to be efficient, reaching 98.8% efficiency at rated load. The higher the switching frequency, the greater the discrepancy between the performance of SiC and SiC-Cascode devices. This caused due to switching losses which is more significant using SiC devices.

During operation at higher switching frequency, the rise and fall times of the V_{DS} voltage were measured, as seen in Figure 10. As expected, a difference between the switching times was verified, with the SiC-cascode device being faster in the transitions. Due to this feature, the overlap time between current and voltage is reduced, causing less switching power loss, and achieving greater overall efficiency. This occurs due to the simplified characteristics of the activation of the SiC-Cascode switch, with reduced output capacitance (C_{oss}) of the transistor at rated DC-bus voltage (400 V), being 32 pF against 52 pF of the SiC switch, approximately. Therefore, for both technologies, reduced switching times were observed, which lead to lower power switching loss. This characteristic highlights the importance of the article presented herein for the advancement of MEA since it demonstrates that high switching frequencies should be chosen for the design of DC-DC conversion systems with reduced weight, leading to the reduction of fuel consumption in the aircraft.

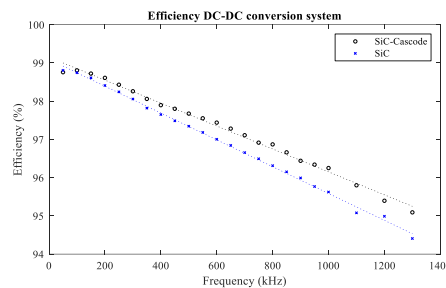


Figure 9. Efficiency x Frequency, DC-DC conversion system

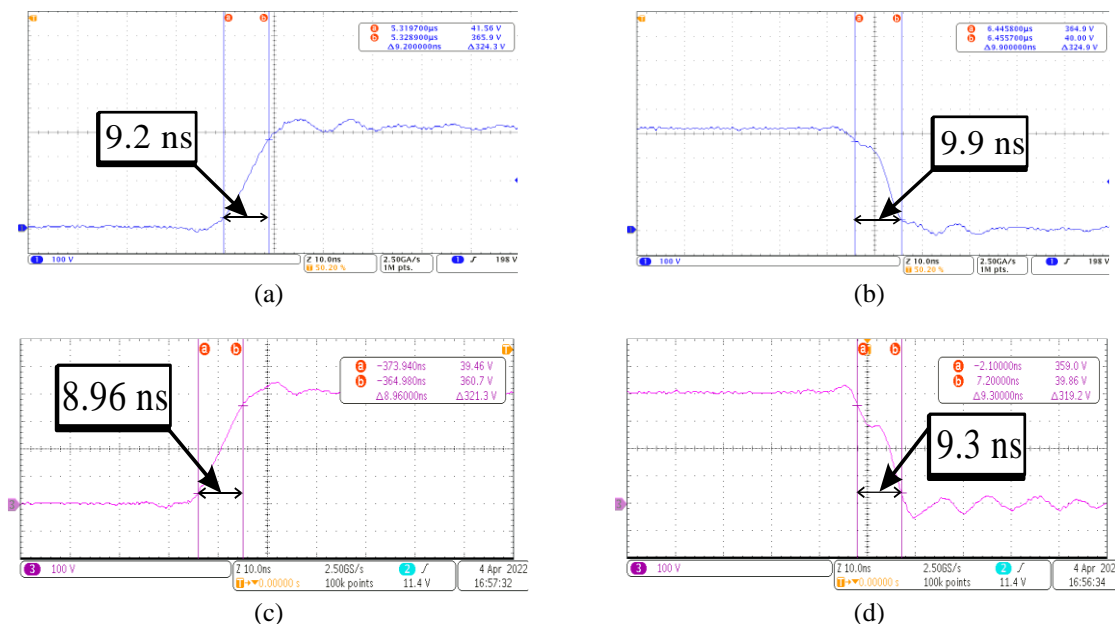


Figure 10. Experimental results; switching time for SiC MOSFET: (a) rise time and (b) fall time: switching time for SiC-Cascode MOSFET, (c) rise time, and (d) fall time

4.2. AC-DC conversion system for MEA

Figure 11 shows the main waveforms observed in the laboratory with AC power supply frequency of 400 Hz and 800 Hz and switching frequency of 200 kHz. The waveforms were acquired from the TEKTRONIX MDO3034 and MDO4054-3 oscilloscopes, together with the TEKTRONIX TPCA-300 current sensor. The data for measuring harmonic distortion were obtained from oscilloscopes, with a sampling of 1 Msamples/s, stored in an external device and processed computationally via MATLAB. Up to the 41st harmonic orders were considered, and data equivalent to three fundamental periods sampled in each case were treated.

For both AC power supply frequencies, low harmonic distortion of current and high-power factor is achieved. From the analyses of the waveforms, it is also possible to observe that there is more significant distortion in the voltage and current waveforms when SiC-Cascode device is used. This arises from the high dv/dt indexes inserted by the fast-switching technology, but can be mitigated by raising the drive resistors, with a consequent reduction in the switching speed and efficiency [2]. This feature sets up a conflict of choice between distortion minimization and circuit efficiency, and it is up to the designer to find the optimal operating point, which changes according to the technology deployed. This difference, although subtle, can lead to problems with EMI, and should be explored through practical analysis in future works.

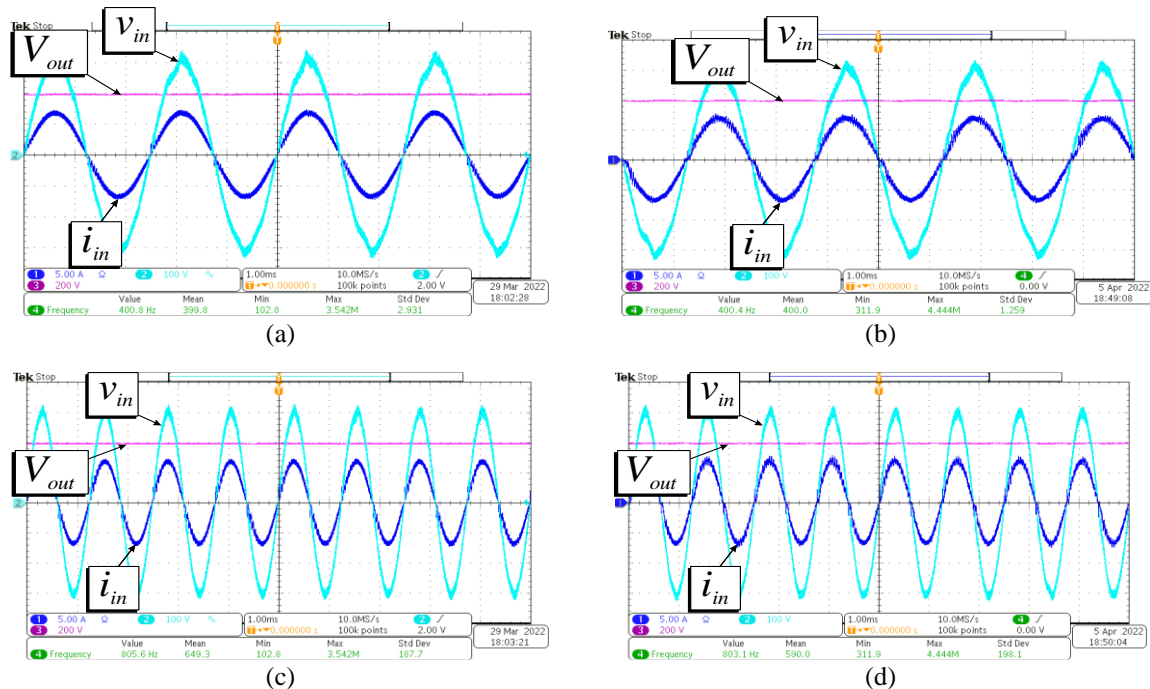


Figure 11. Waveforms, MEA AC-DC operation with 400 Hz: (a) SiC MOSFET, (b) SiC-Cascode MOSFET, (c) SiC MOSFET, and (d) SiC-Cascode MOSFET

For the efficiency analysis, the results presented herein were obtained varying the switching frequency between 100 kHz and 1000 kHz. Figure 12 demonstrates that better results are achieved with the SiC-Cascode device. Peak efficiency for AC power supply frequency of 400 Hz was achieved at 100 kHz switching frequency, reaching 98.12%, against 98.00% obtained with SiC device. For the higher analyzed switching frequency (1000 kHz), the SiC-Cascode technology proved to be superior, with 96.2% efficiency against 94.93% achieved with the SiC technology. Such a reduction in efficiency, compared to DC-DC conversion system, comes from the insertion of the diode rectifier bridge at the input of the circuit, which causes additional power losses. For operation with AC power supply frequency at 800 Hz, the results are similar.

Figure 13 presents the main obtained results for a wide load range and with 400 Hz AC power supply frequency and 250 kHz switching frequency. With SiC-Cascode device the achieved efficiency level is higher when compared to results obtained with SiC device. For the power factor, measured from YOKOGAWA WT230 precision equipment, the results obtained remained above 0.96 for both technologies,

increasing according to the load level and reaching a peak value above 0.99 at rated load. Due to faster switching conditions, SiC-Cascode technology introduces more noise into the system as observed in Figure 11, leading to a slight variation in the achieved power factor. Consequently, a degradation in the harmonic distortion index of the input current can be observed for this technology, with about 16% of distortion for the lowest load condition (22% of the rated power), decreasing to 5% at rated power. In contrast, SiC technology did not present such problems, providing a THDi of 7% for the lowest load condition and 2% at rated power.

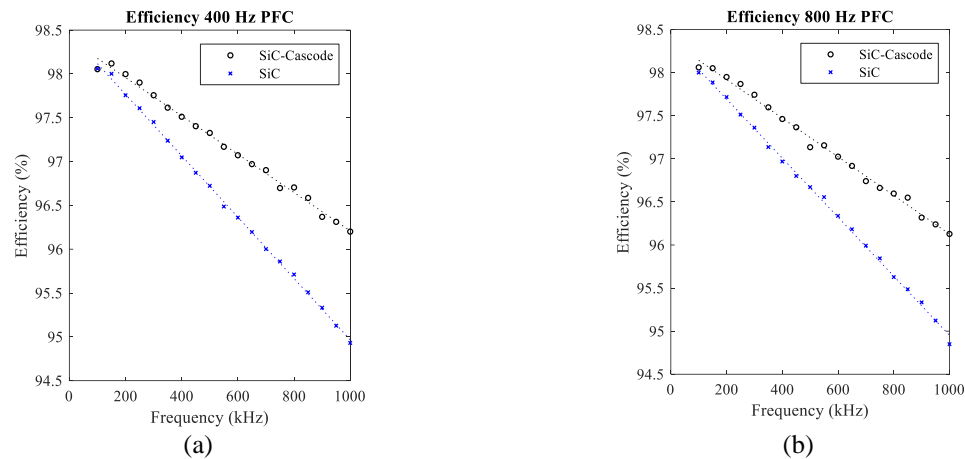


Figure 12. Efficiency x frequency, AC-DC operation with different AC power supply frequency: (a) 400 Hz and (b) 800 Hz

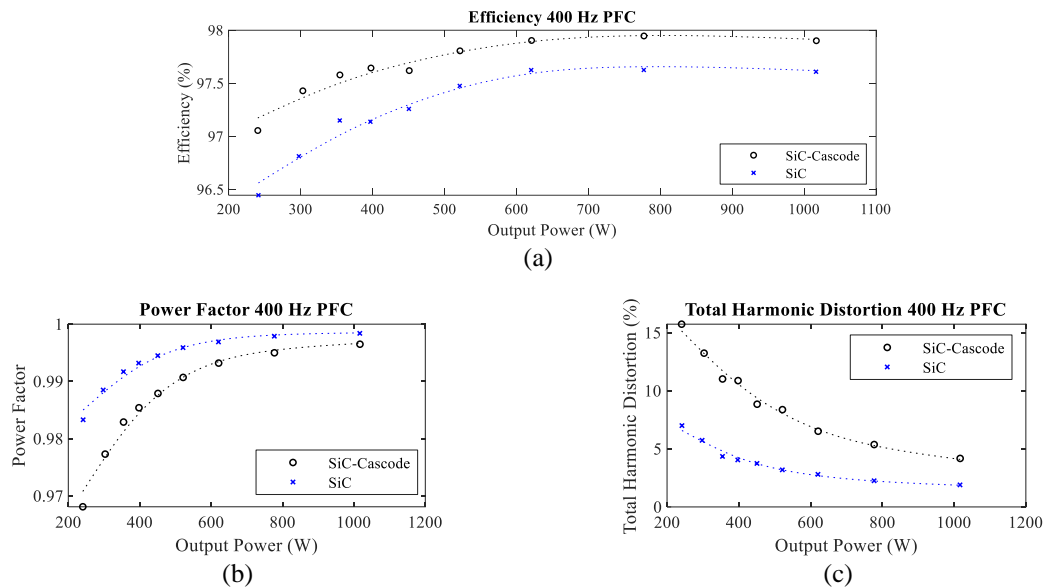


Figure 13. Experimental results for wide load range with 400 Hz AC power supply frequency: (a) efficiency, (b) power factor, and (c) total harmonic distortion of the input line current

With 800 Hz AC power supply frequency, the results obtained at rated load confirm a THDi of about 3% (SiC) and 5% (SiC-Cascode), and power factor above 0.99. As the 800 Hz AC power supply frequency is used sporadically in aircraft systems, the results for different load conditions will be analyzed only at nominal AC power supply frequency (400 Hz). The dynamic response of the output voltage controller and the Boost input current controller, when subjected to a 50% load step down and over, can be seen from Figure 14. They resulted in settling times of about 60 ms under both applied conditions, and percentage overshoot/undershoot of approximately 7% during dynamic tests.

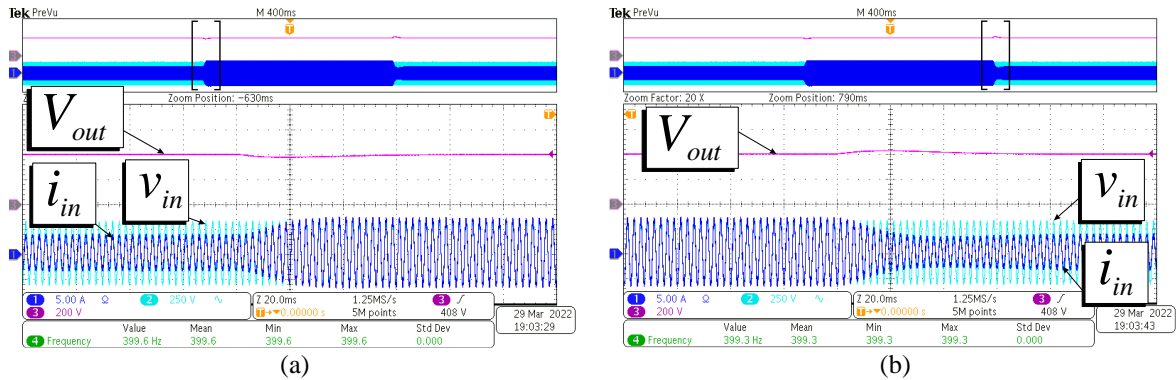


Figure 14. Dynamic response at 400 Hz (200 V/div, 5 A/div, and 20 ms/div):

(a) load step from 50% to 100% of rated power and (b) load step from 50% to 100% of rated power

As a specific condition found in MEA systems, the dynamic variation of the input voltage frequency was also addressed. Applying an increasing voltage frequency ramp from 400 Hz to 800 Hz, during 200 ms, it is possible to observe that the SOGI-PLL operation accurate. The system was able to follow the frequency variation, keeping the imposition of the input current synchronized with the ac voltage. The output voltage remained regulated at 400 V throughout the entire transient period, validating the voltage regulation for the frequency ramp. Figure 15 shows the behavior of the structure facing variation of the grid power supply frequency, proving that a perfect synchronism between current and voltage is achieved. As observed, the system was able to maintain synchronism under frequency variation, maintaining power factor correction and load voltage regulation.

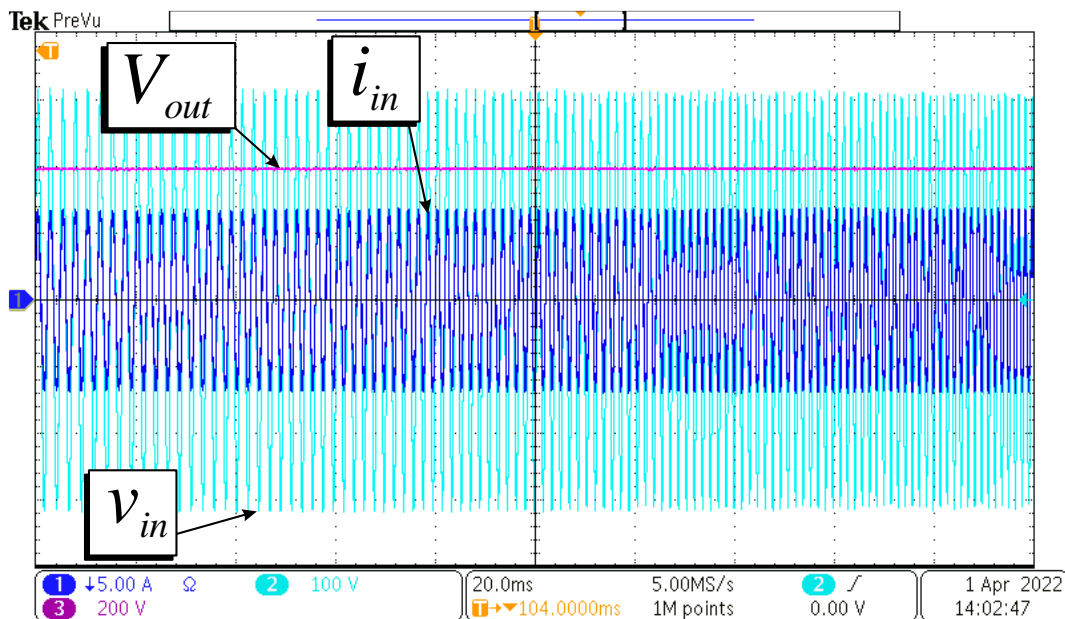


Figure 15. Synchronism between grid voltage and current during frequency variation (from the left to the right: from 400 Hz to 800 Hz, during 200 ms)

5. CONCLUSIONS

The mathematical description of power losses in power electronics converters deploying SiC and SiC-Cascode devices is described in this paper, and it was corroborated by experimental analysis. It has been demonstrated that Wide-bandgap semiconductors can achieve high switching speed and high efficiency even at switching frequencies above 1.0 MHz. Both technologies provide reduced switching times, which lead to lower power switching loss. This characteristic highlights the importance of the article presented herein for

the advancement of More Electric Aircraft, since it demonstrates that high switching frequencies should be chosen for the design of DC-DC and AC-DC conversion systems with reduced weight, leading to the reduction of fuel consumption in the aircraft.

For DC-DC conversion systems, the SiC-Cascode MOSFET has simplified drive characteristics, with lower gate-driver requirement, since lower level of peak current is needed. With SiC-Cascode device, the main differences are found in the power switching loss and the power conduction loss. For 100 kHz switching frequency, the power switching losses are equivalent to only 10% of the total power loss; while at 500 kHz, the total power loss is equivalent to 42%, with linear growth as the switching frequency increases. The reduction in the power switching losses is due to the simplification of the transistor's drive characteristics, which has higher V_{TH} and lower V_{PL} , leading to a shorter current transition period and waveforms overlap. In this context, it is important to emphasize that this operational characteristic together with the intrinsic capacitance values, dictate the switching speeds, directly affecting the bandwidth of the transistor. Therefore, special attention must be dedicated when choosing FETs for designs with high switching frequency.

On the other hand, for AC-DC conversion systems, SiC-Cascode technology introduces more noise into the system, leading to a significant degradation in the harmonic distortion index of the input current. This arises from the high dv/dt indexes inserted by the fast-switching technology, but can be mitigated by raising the drive resistors, with a consequent reduction in the switching speed and efficiency. This feature sets up a conflict of choice between distortion minimization and circuit efficiency, and it is up to the designer to find the optimal operating point, which changes according to the technology deployed. The difference in THDi, although subtle, can lead to problems with EMI, and should be explored through practical analysis in future work. In this context, the THDi achieved was above 5% for a wide load range. For the lowest load condition (22% of the rated power), a THDi of 16% was observed, decreasing to 5% at rated power. In contrast, SiC technology did not present such problems, providing a THDi of 7% for the lowest load condition and 2% at rated power. Therefore, since SiC technology presents greater stability in its parameters, lower EMI irradiation can be assured using this device. In conclusion, one can observe that SiC and SiC-Cascode devices can provide high efficiency and high-power density to energy conversion systems found in MEA's Electric Power Systems. However, the commutation speed of semiconductors must be carefully analyzed in order to reach the optimal relation between EMI and efficiency.

ACKNOWLEDGEMENTS

This research was partially financed by National Council for Scientific and Technological Development (CNPq) under grants 303350/2019-9 and 147857/2021-0; the Coordination for the Improvement of Higher Education Personnel (CAPES); the Research Support Foundation of the State of Minas Gerais (FAPEMIG) under grant PPM-00485-17, and the Federal University of Uberlandia (UFU), under process 23117.060675/2022-10. The authors would like to thank Texas Instruments for the ICs samples, and Professors João B. Vieira Junior and Luiz C. Freitas for supporting this work through grants 304489/2017-4 and 304479/2017-9 of the National Council for Scientific and Technological Development (CNPq).

REFERENCES




- [1] V. Benda, N. Barsoum, J. F. Webb, and P. Vasant, "Power semiconductors—state of art and future trends," Sarawak, (Malaysia), 2011, pp. 16–24. doi: 10.1063/1.3592437.
- [2] X. Yuan, I. Laird, and S. Walder, "Opportunities, Challenges, and Potential Solutions in the Application of Fast-Switching SiC Power Devices and Converters," *IEEE Trans. Power Electron.*, vol. 36, no. 4, pp. 3925–3945, Apr. 2021, doi: 10.1109/TPEL.2020.3024862.
- [3] J. Millan, P. Godignon, X. Perpina, A. Perez-Tomas, and J. Rebollo, "A Survey of Wide Bandgap Power Semiconductor Devices," *IEEE Trans. Power Electron.*, vol. 29, no. 5, pp. 2155–2163, May 2014, doi: 10.1109/TPEL.2013.2268900.
- [4] R. Ø. Nielsen, L. Török, S. Munk-Nielsen, and F. Blaabjerg, "Efficiency and cost comparison of Si IGBT and SiC JFET isolated DC/DC converters," in *IECON 2013 - 39th Annual Conference of the IEEE Industrial Electronics Society*, Nov. 2013, pp. 695–699. doi: 10.1109/IECON.2013.6699219.
- [5] M. G. H. Aghdam and T. Thiringer, "Comparison of SiC and Si power semiconductor devices to be used in 2.5 kW DC/DC converter," in *2009 International Conference on Power Electronics and Drive Systems (PEDS)*, Nov. 2009, pp. 1035–1040. doi: 10.1109/PEDS.2009.5385745.
- [6] M. Telford, "SiC's power cuts cost," *III-Vs Review*, vol. 16, no. 8, pp. 44–47, Nov. 2003, doi: 10.1016/S0961-1290(03)01182-7.
- [7] B. Zhang and S. Wang, "A survey of EMI research in power electronics systems with wide-bandgap semiconductor devices," *IEEE Journal of Emerging and Selected Topics in Power Electronics*, vol. 8, no. 1, pp. 626–643, Mar. 2020, doi: 10.1109/JESTPE.2019.2953730.
- [8] P. Bogóñez-Franco and J. B. Sendra, "EMI comparison between Si and SiC technology in a boost converter," in *International Symposium on Electromagnetic Compatibility - EMC EUROPE*, Sep. 2012, pp. 1–4. doi: 10.1109/EMCEurope.2012.6396739.
- [9] A. M. S. Al-bayati, S. S. Alharbi, S. S. Alharbi, and M. Matin, "A comparative design and performance study of a non-isolated DC-DC buck converter based on Si-MOSFET/Si-Diode, SiC-JFET/SiC-schottky diode, and GaN-transistor/SiC-Schottky diode

- power devices,” in *2017 North American Power Symposium (NAPS)*, Morgantown, WV, Sep. 2017, pp. 1–6. doi: 10.1109/NAPS.2017.8107192.
- [10] B. Rubino, G. Catalisano, L. Abbatelli, and S. Buonomo, “Comparative analysis of driving approach and performance of 1.2 kV SiC MOSFETs, Si IGBTs, and normally-off SiC JFETs,” *STMicroelectronics*, 2015. Accessed: Apr. 27, 2022. [Online]. Available: https://www.st.com/resource/en/technical_article/ta0349-comparative-analysis-of-driving-approach-and-performance-of-12-kv-sic-mosfets-si-igbt-and-normallyoff-sic-jfets-stmicroelectronics.pdf
 - [11] R. M. Burkart and J. W. Kolar, “Comparative evaluation of SiC and Si PV inverter systems based on power density and efficiency as indicators of initial cost and operating revenue,” in *2013 IEEE 14th Workshop on Control and Modeling for Power Electronics (COMPEL)*, Jun. 2013, pp. 1–6. doi: 10.1109/COMPEL.2013.6626462.
 - [12] M. M. Swamy, J.-K. Kang, and K. Shirabe, “Power loss, system efficiency, and leakage current comparison between Si IGBT VFD and SiC FET VFD with various filtering options,” *IEEE Trans. on Ind. Applicat.*, vol. 51, no. 5, pp. 3858–3866, Sep. 2015, doi: 10.1109/TIA.2015.2420616.
 - [13] O. M. Rodríguez-Benítez *et al.*, “Comparative performance and assessment study of a current-fed DC-DC resonant converter combining Si, SiC, and GaN-based power semiconductor devices,” *Electronics*, vol. 9, no. 11, p. 1982, Nov. 2020, doi: 10.3390/electronics9111982.
 - [14] F. M. Shah, S. Maqsood, R. Damaševičius, and T. Blažauskas, “Disturbance rejection and control design of MVDC converter with evaluation of power loss and efficiency comparison of SiC and Si based power devices,” *Electronics*, vol. 9, no. 11, p. 1878, Nov. 2020, doi: 10.3390/electronics9111878.
 - [15] M. F. Yaakub, M. A. M. Radzi, F. H. M. Noh, and M. Azri, “Silicon carbide power device characteristics, applications and challenges: an overview,” *IJPEDS*, vol. 11, no. 4, p. 2194, Dec. 2020, doi: 10.11591/ijpeds.v11.i4.pp2194-2202.
 - [16] S. Bhattacharya, C. Willich, and J. Kallo, “Design and Demonstration of a 540 V/28 V SiC-Based Resonant DC–DC Converter for Auxiliary Power Supply in More Electric Aircraft,” *Electronics*, vol. 11, no. 9, p. 1382, Apr. 2022, doi: 10.3390/electronics11091382.
 - [17] W. Alves, L. Morais, and P. Cortizo, “Design of an highly efficient AC-DC-AC three-phase converter using SiC for UPS applications,” *Electronics*, vol. 7, no. 12, p. 425, Dec. 2018, doi: 10.3390/electronics7120425.
 - [18] B. Hanko, M. Frivaldsky, and J. Morgos, “Evaluation of the efficiency performance of 3-phase, 6-switch PFC circuit based on the used 1.2 kV SiC transistor,” *Electronics*, vol. 11, no. 3, p. 363, Jan. 2022, doi: 10.3390/electronics11030363.
 - [19] M. R. Rogina, A. Rodríguez, A. Vázquez, D. G. Lamar, and M. M. Hernando, “Event-focused digital control to keep high efficiency in a wide power range in a SiC-based synchronous DC/DC boost converter,” *Electronics*, vol. 9, no. 12, p. 2154, Dec. 2020, doi: 10.3390/electronics9122154.
 - [20] J. Rąbkowski, A. Łasica, M. Zdanowski, G. Wrona, and J. Starzyński, “Portable DC supply based on SiC power devices for high-voltage Marx generator,” *Electronics*, vol. 10, no. 3, p. 313, Jan. 2021, doi: 10.3390/electronics10030313.
 - [21] R. Kopacz, M. Harasimczuk, B. Lasek, R. Miśkiewicz, and J. Rąbkowski, “All-SiC ANPC submodule for an advanced 1.5 kV EV charging system under various modulation methods,” *Energies*, vol. 14, no. 17, p. 5580, Sep. 2021, doi: 10.3390/en14175580.
 - [22] C.-T. Ma and Z.-H. Gu, “Review of GaN HEMT applications in power converters over 500 W,” *Electronics*, vol. 8, no. 12, p. 1401, Nov. 2019, doi: 10.3390/electronics8121401.
 - [23] M. J. Carra, H. Tacc, and J. Lipovetzky, “Performance evaluation of GaN and Si based driver circuits for a SiC MOSFET power switch,” *IJPEDS*, vol. 12, no. 3, p. 1293, Sep. 2021, doi: 10.11591/ijpeds.v12.i3.pp1293-1303.
 - [24] “GAN-HIGHPOWER,” *GaN-Highpower / Hochschule Bonn-Rhein-Sieg (H-BRS)*, 2021. <https://www.h-brs.de/de/gan-highpower> (accessed May 01, 2022).
 - [25] J. Bendel, “Cascode configuration eases challenges of applying SiC JFETs,” United Silicon Carbide, Inc., Mar. 2016. Accessed: Apr. 27, 2022. [Online]. Available: https://unitedsic.com/appnotes/USCi_AN0004-Cascode-Configuration-Eases-Challenges-of-Applying-SiC-JFETs.pdf
 - [26] K. Ni *et al.*, “Electrical and Electronic Technologies in More-Electric Aircraft: A Review,” *IEEE Access*, vol. 7, pp. 76145–76166, 2019, doi: 10.1109/ACCESS.2019.2921622.
 - [27] H. Schefer, L. Fauth, T. H. Kopp, R. Mallwitz, J. Friebe, and M. Kurrat, “Discussion on electric power supply systems for all electric aircraft,” *IEEE Access*, vol. 8, pp. 84188–84216, 2020, doi: 10.1109/ACCESS.2020.2991804.
 - [28] B. Karanayil, M. Ciobotaru, and V. G. Agelidis, “Power flow management of isolated multiport converter for more electric aircraft,” *IEEE Trans. Power Electron.*, vol. 32, no. 7, pp. 5850–5861, Jul. 2017, doi: 10.1109/TPEL.2016.2614019.
 - [29] J. Chen, C. Wang, and J. Chen, “Investigation on the selection of electric power system architecture for future more electric aircraft,” *IEEE Trans. Transp. Electrific.*, vol. 4, no. 2, pp. 563–576, Jun. 2018, doi: 10.1109/TTE.2018.2792332.
 - [30] “C3D10065A Datasheet,” Cree, Inc., Dec. 2015.
 - [31] D. Marroqui, A. Garrigos, J. M. Blanes, R. Gutierrez, E. Maset, and F. Iannuzzo, “SiC MOSFET vs SiC/Si Cascode short circuit robustness benchmark,” *Microelectronics Reliability*, vol. 100–101, p. 113429, Sep. 2019, doi: 10.1016/j.microrel.2019.113429.
 - [32] C. Zhao, L. Wang, X. Yang, F. Zhang, and Y. Gan, “Comparative investigation on paralleling suitability for SiC MOSFETs and SiC/Si Cascode Devices,” *IEEE Trans. Ind. Electron.*, vol. 69, no. 4, pp. 3503–3514, Apr. 2022, doi: 10.1109/TIE.2021.3070519.
 - [33] S. Martin, T. Kayiranga, Y. Shi, and H. Li, “Comparative study of a 100kW PV WBG inverter using 1200V SiC MOSFET and JFET cascode devices,” in *2018 IEEE Applied Power Electronics Conference and Exposition (APEC)*, San Antonio, TX, Mar. 2018, pp. 399–405. doi: 10.1109/APEC.2018.8341042.
 - [34] B. Vasilev, “Analysis and improvement of the efficiency of frequency converters with pulse width modulation,” *IJECE*, vol. 9, no. 4, p. 2314, Aug. 2019, doi: 10.11591/ijece.v9i4.pp2314-2320.
 - [35] S. Suroso, D. T. Nugroho, A. N. Azis, and T. Noguchi, “Simplified five-level voltage source inverter with level-phase-shifted carriers based modulation technique,” *IJECS*, vol. 13, no. 2, p. 461, Feb. 2019, doi: 10.11591/ijeecs.v13.i2.pp461-468.
 - [36] E. L. Carvalho, L. H. Meneghetti, E. G. Carati, J. P. da Costa, C. M. de O. Stein, and R. Cardoso, “Asymmetrical pulse-width modulation strategy for current-fed dual active bridge bidirectional isolated converter applied to energy storage systems,” *Energies*, vol. 13, no. 13, p. 3475, Jul. 2020, doi: 10.3390/en13133475.
 - [37] M. Shahab, S. Wang, and A. K. Junejo, “Improved control strategy for three-phase microgrid management with electric vehicles using multi objective optimization algorithm,” *Energies*, vol. 14, no. 4, p. 1146, Feb. 2021, doi: 10.3390/en14041146.
 - [38] N. A. Rai, M. J. A. Aziz, M. R. Sahid, and S. Md. Ayob, “Bridgeless PFC single ended primary inductance converter in continuous current mode,” *IJPEDS*, vol. 10, no. 3, p. 1427, Sep. 2019, doi: 10.11591/ijpeds.v10.i3.pp1427-1436.
 - [39] J. L. Afonso *et al.*, “A Review on Power Electronics Technologies for Power Quality Improvement,” *Energies*, vol. 14, no. 24, p. 8585, Dec. 2021, doi: 10.3390/en14248585.




- [40] S. Prakash, J. K. Singh, R. K. Behera, and A. Mondal, "Comprehensive analysis of SOGI-PLL based algorithms for single-phase system," in *2019 National Power Electronics Conference (NPEC)*, Tiruchirappalli, India, Dec. 2019, pp. 1–6. doi: 10.1109/NPEC47332.2019.9034724.
- [41] N. S. Nise, *Control systems engineering*, 6th ed. Hoboken, NJ: Wiley, 2011.
- [42] E. O. Prado, P. C. Bolsi, H. Confortin Sartori, and J. Renes Pinheiro, "Analytical model for the calculation of losses in power mosfets for database applications," *REP*, vol. 26, no. 04, pp. 388–398, Dec. 2021, doi: 10.18618/REP.2021.4.0023.
- [43] C. W. T. McLyman, *Transformer and inductor design handbook*, 3rd ed., rev. Expanded. New York: Marcel Dekker, 2004.

BIOGRAPHIES OF AUTHORS






Osmar Felipe Alves Eleodoro    was born in Alta Floresta, Brazil, in 1999. He is currently pursuing a M.Sc degree in Electrical Engineering at the Research Center in Power Electronics (NUPEP) of the Federal University of Uberlândia (UFU). His areas of interest are: Wide-bandgap semiconductor applications, switched converters, electric vehicles, and digital control applied to power electronics. He can be contacted at email: osmareleodoro@yahoo.com.






Vitor Fonseca Barbosa    holds a B.Sc degree from the Federal University of Triângulo Mineiro (UFTM) and an M.Sc degree from the Federal University of Uberlândia (UFU) in 2017 and 2020, respectively. He is currently pursuing a Ph.D in Electrical Engineering at the of the Research Center in Power Electronics (NUPEP) at UFU. His areas of interest are: active power factor correction, digital signal processing, switched converters, hybrid rectifiers, DC microgrids and more electric aircraft (MEA). He can be contacted at email: vitorfonsecabarbosa@gmail.com.



Gustavo B. Lima    was born in Ibiassucê, Brazil, in 1986. Received the B.Sc., M.Sc., and Ph.D. degrees in electrical engineering from the Universidade Federal de Uberlândia, Uberlândia, MG, Brazil, in 2010, 2012, and 2015, respectively. He is currently with the Research Center in Power Electronics (NUPEP) at UFU and since 2017 he has been a professor member. His research interests include hybrid rectifiers, digital control applied to power electronics and power factor correction. He can be contacted at email: gustavo.brito.28@ufu.br.



Luiz Carlos Gomes Freitas    was born in Uberlândia, Brazil, in 1976. Graduated in Electrical Engineering with emphasis on Power Systems from the Federal University of Uberlândia (2001), master's degree (2003) and Ph.D (2006) in Electrical Engineering with emphasis on Power Electronics from the same university. In his doctoral thesis he developed an innovative topological design of a three-phase hybrid rectifier for high power drive systems. In 2012, he received the 2nd Prize Paper Award of the IEEE-IAS-Industrial Automation and Control Committee (IACC) for his contribution to the development of hybrid rectifier structures. In 2008 he joined the faculty of the Federal University of Uberlândia where he has been working developing teaching and research activities in the area of Power Electronics and Power Systems. Since 2010 he has been the coordinator of the Research Center in Power Electronics (NUPEP) at UFU. Since 2013 he has been a researcher recognized by National Council for Scientific and Technological Development (CNPq) with a research productivity grant. he has experience in the area of electrical engineering, with an emphasis on conversion and rectification of electric energy, working on various topics related to power electronics, electric power quality and renewable energy. He can be contacted at email: lcgfreitas@ufu.br.